ELSEVIER

Journal of Atmospheric and Solar-Terrestrial Physics 66 (2004) 1257–1270

Journal of ATMOSPHERIC AND SOLAR-TERRESTRIAL PHYSICS

www.elsevier.com/locate/jastp

The photospheric boundary of Sun-to-Earth coupled models

W.P. Abbett[a,*], Z. Mikić[b], J.A. Linker[b], J.M. McTiernan[a], T. Magara[a,c], G.H. Fisher[a]

[a]*Space Sciences Laboratory, University of California, Berkeley, CA 94720-7450, USA*
[b]*Science Applications International Corporation, 10260 Campus Point Dr., San Diego, CA 92121-1578, USA*
[c]*Naval Research Laboratory, Code 7675, Washington DC 20375-2352, USA*

Received 23 January 2004; received in revised form 5 March 2004; accepted 12 March 2004
Available online 5 August 2004

Abstract

The least understood component of the Sun-to-Earth coupled system is the solar atmosphere—the visible layers of the Sun that encompass the photosphere, chromosphere, transition region and low corona. Coronal mass ejections (CMEs), principal drivers of space weather, are magnetically driven phenomena that are thought to originate in the low solar corona. Their initiation mechanism, however, is still a topic of great debate. If we are to develop physics-based models with true predictive capability, we must progress beyond simulations of highly idealized magnetic configurations, and develop the techniques necessary to incorporate observations of the *vector* magnetic field at the solar photosphere into numerical models of the solar corona. As a first step toward this goal, we drive the SAIC coronal model with the complex magnetic fields and flows that result from a sub-photospheric MHD simulation of an emerging active region. In particular, we successfully emerge a twisted Ω-loop into a pre-existing coronal arcade.

To date, it is not possible to directly measure the magnetic field in the solar corona. Instead, we must rely on non-potential extrapolations to generate the twisted, pre-eruptive coronal topologies necessary to initiate data-driven MHD simulations of CMEs. We therefore investigate whether a non-constant-α force-free extrapolation can successfully reproduce the magnetic features of a self-consistent MHD simulation of flux emergence through a stratified model atmosphere. We generate force-free equilibria from simulated photospheric and chromospheric vector magnetograms, and compare these results to the MHD calculation. We then apply these techniques to an IVM (Mees Solar Observatory) vector magnetogram of NOAA active-region 8210, a source of a number of eruptive events on the Sun.

Keywords: Methods; Numerical; MHD; Sun; Photosphere; Magnetic fields; Corona

1. Introduction

Soft X-ray images of the solar corona suggest that coronal mass ejections (CMEs) tend to arise in connection with active regions exhibiting sheared and or twisted coronal loops called sigmoids (Canfield et al., 1999). It is understood that these features are signs of stressed magnetic fields containing free energy that can be released by simple evolution, by some destabilizing event such as local emergence of new magnetic flux from below the photosphere, or by changes in magnetic connectivity due to events elsewhere on the Sun (see e.g., Feynman and Martin, 1995; Antiochos et al., 1999). CME modeling endeavors such as those of The Center for Integrated Space Weather Modeling (CISM) and the

*Corresponding author. Tel. +1-510-642-6880.
E-mail address: abbett@ssl.berkeley.edu (W.P. Abbett).

1364-6826/$ - see front matter
doi:10.1016/j.jastp.2004.03.016

solar Multi-University Research Initiative (MURI; the DoD/AFOSR funded project entitled "Understanding Magnetic Eruptions and their Interplanetary Consequences") must therefore overcome both the problem of self-consistently incorporating photospheric magnetic fields and flows into the lower boundary of dynamic models of the corona (see e.g., Welsch et al., 2004), and the problem of initiating these simulations with realistic, potentially eruptive active-region topologies.

To date, there is no way to directly measure the magnetic field in the corona (though there is steady progress in this area, see Kuhn et al., 1999; Lin et al., 2000; Casini et al., 2003; Tomczyk, 2003). While it is possible to infer the magnetic topology of the corona from a careful analysis of emission in various broad or narrow band passes (e.g. Yohkoh and TRACE data, respectively), it is often difficult to obtain an unambiguous, detailed interpretation of the data suitable for incorporation into a numerical model. At present, the most widely used means to infer the magnetic structure of the solar corona is to use line-of-sight full- or partial-disk photospheric magnetograms (measurements of the field strength at the visible surface of the Sun) as a basis for a potential field or force-free extrapolation; the derived magnetic topologies are then compared with observations of coronal emission.

Of the two extrapolation methods, the global potential field source surface (PFSS) model (see e.g., Luhmann et al., 2002 and references therein) is less computationally expensive. The magnetic field is assumed to be radial at an outer spherical boundary (the "source surface"), and potential within a spherical shell (with the lower boundary anchored at the photosphere). While the PFSS model provides an estimate of the global topology in the absence of transient events, it has limitations in and around active regions, where the solar atmosphere is significantly non-potential. Both global and local force-free extrapolations (see e.g., Amari et al., 1997; McClymont et al., 1997; Wheatland et al., 2000; Liu et al., 2002; Bleybel et al., 2002; Régnier et al., 2002), can provide an improved representation of active region magnetic structures in the low-β, highly conducting plasma of the low corona. In this approximation, $\mathbf{J} \times \mathbf{B} \equiv 0$ (here, $\mathbf{J}$ and $\mathbf{B}$ have the standard definitions of current density and magnetic field, respectively, and β represents the ratio of the gas to magnetic pressure), thus the current density and magnetic field are parallel, and can be expressed as $\mathbf{J} = 4\pi\alpha\mathbf{B}$. If the coefficient α is assumed constant throughout the volume, then the problem becomes linear, and the solution is relatively straightforward and computationally inexpensive to perform; however, if α is allowed to vary across field lines (a non-constant-α force-free extrapolation), the mathematical problem becomes non-linear. The existence of the solution of this difficult non-linear problem and the nature of the boundary conditions that make it well-posed are currently an active research topic (e.g., see Schmidt, 1964; Bineau, 1972; Aly, 1991; Amari et al., 1997).

Both the PFSS and force-free methods give static representations of the state of the solar corona at a given instant. However, to study initiation mechanisms of eruptive events such as CMEs, and to continuously follow the time evolution of the solar atmosphere, a dynamic model is required. MHD models provide a means to characterize the topological evolution of the solar corona, and can provide information on how fields reconnect, though certain simplifying assumptions (particularly in the treatment of the energetics) are often required to make the problem numerically tractable. Our region of interest, the solar atmosphere (the combined layers of the photosphere, chromosphere, transition region, and low corona), is notoriously difficult to model: the domain spans many pressure scale heights (requiring grid resolutions of less than ~ 100 km to resolve the photosphere and transition layers while simultaneously simulating large-scale coronal structures), includes both the low-β plasma of the corona, and the $\beta \sim 1$ plasma of the photosphere, includes dynamic regions where energy transport is dominated by radiation and thermal conduction, and in the case of flares and eruptions, can be driven by non-thermal energy deposition and the physics of reconnection at small scales.

Complexities aside, even an idealized dynamic model (e.g., a numerical solution of the ideal MHD system of equations, employing only an approximate treatment of radiation transport) can provide insight into the physics of active-region evolution, and can provide a means to test current theoretical models of CME initiation and evolution (e.g. Forbes and Isenberg, 1991; Antiochos et al., 1999). To date, efforts to model sigmoids either energize initially potential active-region loops by imposing velocity shear at their footpoints (Amari et al., 2003), or emerge twisted magnetic structures from below into regions of a model corona with little or no pre-existing magnetic field (Abbett and Fisher, 2003; Magara and Longcope, 2003; Fan and Gibson, 2003). To progress beyond simulations of such idealized magnetic configurations, it is necessary to develop techniques to drive MHD model coronae with more realistic, complex magnetic fields and flows characteristic of the evolution of pre-eruptive magnetic features observed at the visible surface of the Sun. To address this challenge, we couple the sub-surface model of Abbett et al. (2000, 2001) to the SAIC coronal model (Mikić and Linker, 1994; Linker and Mikić, 1997; Mikić et al., 1999), and emerge a magnetic structure underneath a pre-existing arcade.

Additionally, we use the model of Magara (2004) (a self-consistent 3D MHD simulation of the dynamic emergence of a twisted magnetic flux rope through the stratified layers of the photosphere, chromosphere, and

transition region into the corona) to test methods of initiating MHD models of the pre-eruptive corona with both potential and non-potential field models based on photospheric magnetograms. We then apply these techniques to the observationally obtained vector magnetic field of NOAA active-region 8210 (AR 8210) just prior to a series of eruptive events. The remainder of this paper is organized as follows: In Section 2 we briefly describe the three distinct numerical models used in this study, and describe the realm of applicability of each model. In Section 3 we extend the results of Abbett and Fisher (2003) and demonstrate how a MHD model of the interior can be coupled to the SAIC coronal model when the overlying corona is not field free. In Section 4 we describe our efforts to provide a suitable initial state for an active-region-scale model corona when the system is to be driven by a simulated active region, and apply these techniques to an IVM vector magnetogram of AR 8210. Finally, in Section 5 we summarize our results.

2. Method

We employ a number of numerical methods to both simulate the effect of photospheric magnetic fields and flows on the magnetic topology of the corona, and to test methods of determining initial states and boundary update algorithms for 3D dynamic models of coronal magnetic fields. It remains computationally intractable to simulate the entirety of the solar interior and atmosphere, due in part to the vast difference in characteristic timescales between the interior and the atmosphere, and the very different physical characteristics of the plasma in each respective region (e.g., magnetic field fills the $\beta \ll 1$ corona, while "isolated" flux systems form and evolve within the $\beta \gg 1$ turbulent convection zone). We therefore use three separate numerical models, each designed to efficiently describe one of the three distinct spatial domains: the region below the photosphere (the interior), which is often considered the source of the stressed or twisted active-region fields; the low corona where the pre-eruptive loops reside; and the surface layers, which include the visible photosphere and chromosphere—the layers that necessarily form the inner boundary for MHD models of CMEs.

2.1. The interior

Active regions on the Sun are thought to be the result of the emergence (through the visible surface) of magnetic flux that was generated via dynamo processes deep in the solar interior at or near the base of the solar convection zone, where turbulent layers transition into the stable radiative region. To characterize the complex 3D interaction of magnetically buoyant flux systems (flux tubes and Ω-loops) during their ascent through the convective envelope, and thus to generate realistic sub-surface emerging active regions with self-consistent flow fields that can be used to drive numerical models of the solar atmosphere, we numerically solve the 3D system of MHD equations in the anelastic approximation

$$\nabla\cdot(\rho_0\mathbf{v}) = 0, \tag{1}$$

$$\rho_0\left(\frac{\partial\mathbf{v}}{\partial t} + (\mathbf{v}\cdot\nabla)\mathbf{v}\right) = -\nabla p_1 + \rho_1\mathbf{g} + \frac{1}{4\pi}(\nabla\times\mathbf{B})\times\mathbf{B} + \nabla\cdot\boldsymbol{\Pi}, \tag{2}$$

$$\rho_0 T_0\left(\frac{\partial s_1}{\partial t} + (\mathbf{v}\cdot\nabla)(s_0+s_1)\right) = \nabla\cdot(K\rho_0 T_0\nabla s_1) + \frac{\eta}{4\pi}|\nabla\times\mathbf{B}|^2 + (\boldsymbol{\Pi}\cdot\nabla)\cdot\mathbf{v}, \tag{3}$$

$$\nabla\cdot\mathbf{B} = 0 \tag{4}$$

$$\frac{\partial\mathbf{B}}{\partial t} = \nabla\times(\mathbf{v}\times\mathbf{B}) - \nabla\times(\eta\nabla\times\mathbf{B}), \tag{5}$$

$$\frac{\rho_1}{\rho_0} = \frac{p_1}{p_0} - \frac{T_1}{T_0}, \tag{6}$$

$$\frac{s_1}{c_p} = \frac{T_1}{T_0} - \frac{\gamma-1}{\gamma}\frac{p_1}{p_0}. \tag{7}$$

The anelastic approximation (see e.g., Ogura and Phillips, 1962; Gough, 1969; Lantz and Fan, 1999) results from a scaled variable expansion of the 3D compressible MHD equations about a nearly adiabatically stratified plane-parallel reference atmosphere (which we take to be a polytrope). In the above equations, ρ_1, p_1, T_1, s_1, $\mathbf{v}$, and $\mathbf{B}$ refer to the density, gas pressure, temperature, entropy, velocity, and magnetic field perturbations (for clarity, we drop the "1" subscript on $\mathbf{v}$ and $\mathbf{B}$ so as not to confuse these quantities with the discussion of boundary conditions in Section 3), and ρ_0, p_0, T_0, and s_0 denote the corresponding values of the reference state, taken to be a field-free, nearly adiabatically stratified polytrope of index $m = 1.5$. We note that m is related to the adiabatic index γ by $m \equiv 1/(\gamma-1)$. The viscous stress tensor is given by $\Pi_{ij} \equiv \mu(\partial v_i/\partial x_j + \partial v_j/\partial x_i - 2/3(\nabla\cdot\mathbf{v})\delta_{ij})$, where μ is the coefficient of dynamic viscosity and δ_{ij} is the Kronecker delta function. The remaining parameters in the equations are: $\mathbf{g} = -g\hat{\mathbf{z}}$, the gravitational acceleration (assumed to be uniform); c_p, the specific heat at constant pressure; and η and K, the coefficients of magnetic and thermal diffusion, respectively.

The code ANMHD (Fan et al., 1999; Abbett et al., 2000, 2001) solves the non-dimensional form of the anelastic system of equations in a Cartesian domain assuming periodic boundary conditions in the transverse

directions, and non-penetrating, stress-free conditions at the upper and lower boundaries. In the anelastic approximation, both the magnetic field and momentum density are divergence-free; thus each can be expressed in terms of scalar potentials. These potentials (with the other scalar variables of the system) are spectrally decomposed in the horizontal direction. The Fourier variables are then discretized vertically, and vertical derivatives are approximated by fourth order, centered differences. A semi-implicit method is then used to time-advance the five discretized scalar equations forr the Fourier variables. Using operator splitting, the second-order Adams–Bashforth scheme is applied to the advection terms, and the second-order Crank–Nicholson scheme is applied to the diffusion terms. A detailed description of the numerical methodology used in ANMHD can be found in Appendix A of Fan et al. (1999).

The advantage of the anelastic formulation lies in the computational savings inherent in filtering out fast-moving acoustic waves from the calculation (the time derivative term in the continuity equation is of sufficiently high order in the expansion, and can be neglected). Thus we have the ability to explore a wide range of parameter space using a relatively small amount of CPU time, and can generate a number of complex simulated active regions of various twists, strengths, rotation rates and sizes for incorporation into other models of the solar atmosphere that include photospheric layers. While this approximation is well-suited for simulations of sub-sonic processes in the high-β plasma deep in the convection zone, it breaks down at (and above) the photosphere where β approaches unity. In these regions, a fully compressible treatment is required.

2.2. The surface layers

There are generally two approaches used to model the surface layers of the Sun (the region that begins just below the visible surface and extends through the chromosphere and transition layers). The first is to as realistically as possible model the detailed physics of surface magnetoconvection by including a non-ideal tabular equation of state and solving the radiative transfer equation in detail (see e.g., Bercik, 2002; Stein et al., 2003). This approach allows for a detailed analysis of magnetic fields and surface flows, and the computational results admit to a direct comparison to a variety of observational data, such as emission in granules and intergranular lanes (Stein and Nordlund, 1998). The disadvantage of this approach is that it is computationally expensive, the non-local nature of the radiation field makes these codes difficult to parallelize, and to date the domain size of the calculations have yet to reach active-region spatial scales. Another approach is to simplify the physics, extend the domain to encompass active-region scale features, and study only the evolution of magnetic fields and flows as the plasma transitions from a high-β to low-β regime over the many pressure scale heights of the photosphere, chromosphere, transition region, and corona (Fan, 2001; Magara and Longcope, 2001, 2003).

We adopt the latter approach and use the code of Magara (1998) to solve the fully compressible system of ideal MHD equations in the presence of a (uniform) gravitational field

$$\frac{\partial \rho}{\partial t} + \nabla\cdot(\rho \mathbf{v}) = 0, \tag{8}$$

$$\rho\left(\frac{\partial \mathbf{v}}{\partial t} + (\mathbf{v}\cdot\nabla)\mathbf{v}\right) = -\nabla p + \rho\mathbf{g} + \frac{1}{4\pi}(\nabla \times \mathbf{B}) \times \mathbf{B}, \tag{9}$$

$$\frac{\partial \mathbf{B}}{\partial t} = \nabla \times (\mathbf{v} \times \mathbf{B}), \tag{10}$$

$$\frac{\partial p}{\partial t} + \nabla\cdot(p\mathbf{v}) = -(\gamma - 1)p\nabla\cdot\mathbf{v}. \tag{11}$$

Here, ρ, $\mathbf{v}$, $\mathbf{B}$, p, $\mathbf{g}$, and γ have the standard definitions of gas density, fluid velocity, magnetic field, gas pressure, gravitational acceleration, and adiabatic index ($\gamma = 5/3$ is assumed), respectively. The system of equations is solved in a Cartesian domain using a modified Lax–Wendroff scheme with second-order accuracy both temporally and spatially. The equations are discretized on a non-uniform mesh, with the highest grid concentration in the model transition region, where the gradients in temperature and density are large.

We use the simulations described in Magara (2004) to model the emergence and subsequent evolution of a single, horizontal, highly twisted magnetic flux tube initially positioned just below the model photosphere in a computational domain that spans from ~ 5 Mm below a designated plane at the center of the photospheric layer to the low corona ~ 25 Mm above that plane. This is a fundamentally different type of calculation than that of Abbett and Fisher (2003) (and the calculations presented here in Section 3), where ANMHD model results are used to drive separate MHD model atmospheres. While it is true that including the transition layers in the simulation domain is certainly the most self-consistent means of simulating the emergence of flux from just below the photosphere into the low corona (since there is no arbitrary boundary between individual codes), deeper layers are necessarily excluded, and the flux system that emerges through the model photosphere may not have the same dynamic characteristics as a flux rope that has buoyantly risen through the entirety of a turbulent model convection zone. Further, the solar photosphere represents the lower boundary of Sun to Earth coupled models, and we must assume that we will

have no information available to drive the large-scale coupled system aside from vector magnetic field data obtained at the photosphere via inversions of polarization measurements. Therefore, for the purposes of this study, we will concentrate our efforts on using models of the interior to create simulated magnetograms that will be used to drive models of the solar atmosphere (and to test techniques of incorporating observational data self-consistently into model coronae), and we will use the self-consistent emergence calculation of Magara (2004) principally to test methods of obtaining initial states for initiating coupled calculations.

2.3. The corona

To solve the MHD Eqs. (8)–(11) in a coronal active region, we use a Cartesian coordinate version of the SAIC coronal code. The method of solution (in spherical coordinates) has been described previously (Mikić and Linker, 1994; Linker and Mikić, 1997; Lionello et al., 1999; Mikić et al., 1999; Lionello et al., 2001). The Cartesian version has been used previously in studies using vector magnetograms (Mikić and McClymont, 1994; Lee et al., 1998, 1999), active-region evolution (Mikić et al., 1996), flux emergence (Mok et al., 2001), and prominence formation (Lionello et al., 2002). Briefly, we note that the code uses staggered meshes, which allows us to more easily specify boundary conditions in a self-consistent way. The use of staggered meshes also decouples longitudinal and transverse components of the vector quantities. Thus $\nabla \cdot \mathbf{B} = \nabla \cdot \mathbf{J} = 0$ is satisfied (to within round-off error) for the duration of the calculations.

At this stage, our primary purpose in coupling the ANMHD model of the interior to the SAIC coronal model is to explore the topology and properties of the emergent magnetic field. As the magnetic field energy typically dominates both the plasma kinetic and thermal energies in active regions, we choose to solve a simplified "zero-β" form of Eqs. (8)–(11) (including viscous diffusion), where we assume that $p = 0$, $\mathbf{g} = 0$, and that density ρ is constant throughout the domain. When the system of equations is integrated to a steady state, the solutions represent force-free, non-constant-α solutions for a given set of boundary conditions. This approximation is likely to be quite good for magnetic field configurations that are nearly in equilibrium, but pressure and gravity could influence how the field emerges. Results from this approach can be contrasted with solutions of the full Eqs. (8)–(11) to see how much these processes influence the resulting configuration.

The calculations described here were performed in a box with (x, y, z) dimensions of 2.6×10^5 km by 1.3×10^5 km by 2.6×10^5 km, using $141 \times 111 \times 111$ grid points on a non-uniform mesh. The mesh points were concentrated near the neutral line and the lower boundary; $\Delta z \approx 290$ km near $z = 0$ (the solar surface), and $\Delta x \approx \Delta y \approx 370$ km near the neutral line. A uniform resistivity η has been used, corresponding to a Lundquist number $S = \tau_R/\tau_A = 3 \times 10^4$. Here, $\tau_R = 4\pi L^2/\eta c^2$ is the resistive diffusion time, and $\tau_A = L/v_A$ is the Alfvén time for a length scale $L = 65,000$ km. This is approximately the separation of the two poles of the emerging flux tube (after it has fully emerged). A uniform viscosity ν is also used, corresponding to $\tau_\nu/\tau_A = 150$, where $\tau_\nu = L^2/\nu$ is the viscous diffusion time. The higher viscosity (relative to the resistivity) is useful when relaxing a configuration toward a force-free state.

3. The ANMHD-SAIC combined model

We begin by demonstrating a new code coupling between the sub-surface ANMHD model of the solar interior and the SAIC coronal model. Normally, the term "coupling" refers to a two-way exchange of information from one code to another—for example, two codes with similar characteristic time scales, mesh resolution, and physics can (in principle) be readily coupled together using a message passing framework (see e.g., MacNeice et al., 2000; Lyon et al., 2003). The underlying idea is that at the interface between the two codes, active cells adjacent to the interface of one model are used as the boundary cells of the other, and the calculation proceeds in real time. In our case, the time scales, the physics of the models, and the numerical algorithms of each code are sufficiently dissimilar that such a real time coupling is non-trivial. More importantly, Sun-to-Earth coupled models must terminate at the solar photosphere, since there is currently no way to observationally determine the magnetic structure below the visible surface (aside from helioseismologic inversions) in a manner suitable for driving large scale coupled models. Thus, the photosphere represents the true boundary of a data-driven coupled system, and information transfer across this interface will necessarily be in one direction.

3.1. An initially field-free model corona

A primary reason for exploring this coupling is to develop a robust means of driving fully dynamic MHD model coronae with a time series of magnetic field measurements taken at the photosphere. Therefore, rather than attempting a truly coupled system, we use the sub-surface code ANMHD to provide the boundary conditions to drive the SAIC coronal model. In the case where the corona is initially field-free, this "one-way" coupling is relatively straightforward. Advancement of the equations in the SAIC coronal model requires the specification of the electric field components that are tangential to the boundary ($\mathbf{E}_t = E_x\hat{\mathbf{x}} + E_y\hat{\mathbf{y}}$) and the

velocity normal to $\mathbf{B}$ ($\mathbf{v}_\perp$) at the solar surface $z = 0$ (note that this includes a v_z component). In practice, we supply all three components of $\mathbf{v}$, as $\mathbf{v}_\parallel$ does not affect the zero-β form of Eqs. (8)–(11).

Fig. 1 shows the magnetic field evolution when the models are coupled in this way. The ANMHD code is used to compute the buoyant rise of a twisted flux tube in the solar convection zone, and its intersection with the layers just below the photosphere (Abbett et al., 2000; Abbett and Fisher, 2003). The values of $\mathbf{v}$ and $\mathbf{E}_t$ from this calculation are used as boundary conditions for the coronal evolution, as computed with the SAIC model (we chose to use the data from run SS3 of Abbett et al., 2000, since the flux tube of the calculation is modestly twisted, and does not succumb to the kink instability during its ascent). The electric field used as the boundary condition in the coronal calculation is the "ideal" part of the electric field, $\mathbf{E}_t = -(\mathbf{v} \times \mathbf{B}/c)_t$, with $\mathbf{v}$ and $\mathbf{B}$ extracted from a plane near the top of the simulation domain of the sub-photospheric calculation (i.e., near the photosphere). Red (blue) colors on the solar surface indicate positive (negative) values of B_z. The field lines in Fig. 1 have footpoints chosen randomly to illustrate the topology of the magnetic field. The field emerges with a sheath of non-force-free current surrounding it, and relaxes toward a force-free state inside this sheet.

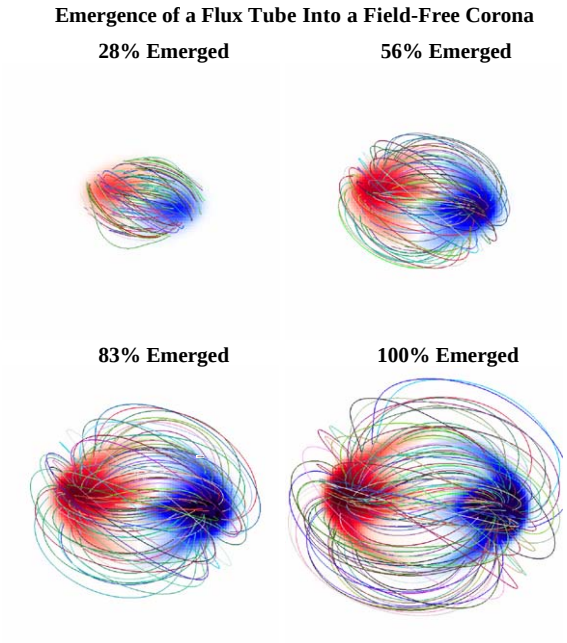

Fig. 1. The evolution of the magnetic field for an initially field-free model corona that is driven from below by the buoyant rise of a modestly twisted magnetic flux rope. The calculation shown uses $141 \times 111 \times 111$ grid points on a non-uniform mesh.

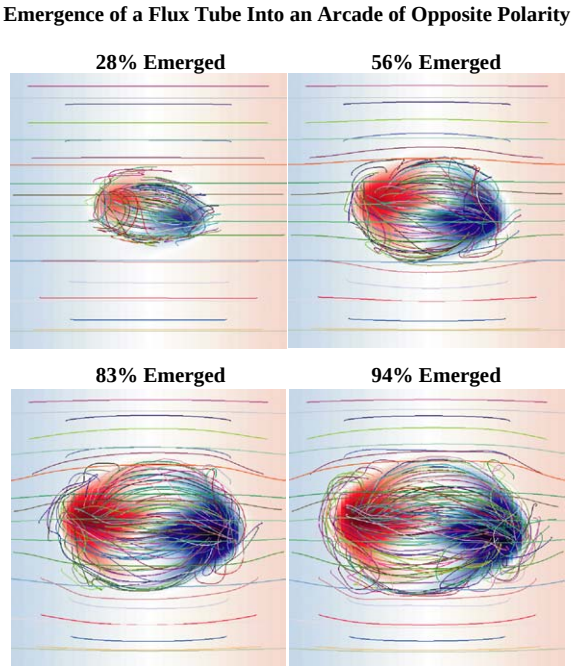

Fig. 2. Magnetic field evolution for a case where active-region magnetic flux emerges into an arcade of opposite polarity. See text for details.

Faraday's law implies that B_z at $z = 0$ evolves strictly due to $\mathbf{E}_t$. Since $\mathbf{E}_t$ is set as a boundary condition on the coronal code from values extracted from the ANMHD code, we expect that B_z at $z = 0$ in the coronal solution should exactly match B_z from the solar interior solution, and we find that this is indeed the case. On the other hand, B_x and B_y arise in part from E_z, which is not specified at the boundary but is computed as part of the solution. Since the high-β regime of the ANMHD solution is far different from the coronal solution, we cannot expect $\mathbf{B}_t$ to match exactly between the two solutions. Nevertheless, we find that qualitatively $\mathbf{B}_t$ is quite similar between the interior and coronal solutions. We note that the magnetic field lines of Fig. 1 compare very well with the magnetic structure shown in Fig. 2 of Abbett and Fisher (2003) (a model corona driven by the same sub-surface evolution), even though the two coronal models are not identical.

3.2. An initial model corona with pre-existing field

Like Abbett and Fisher (2003), the preceding calculation represents a very simple configuration—magnetic flux emerging into a corona with no pre-existing magnetic field. If we now assume that the corona is filled with magnetic field anchored to the photosphere, and use a separate code to introduce additional flux into this system, we must consider how the pre-existing field

interacts with the introduction of new flux when updating the boundary values. There is a fundamental physical inconsistency that arises from the fact that the two distinct codes are not truly "coupled"—the sub-surface code is a completely separate system, and does not self-consistently evolve along with the model corona to the prescribed initial configuration. Although this boundary problem is inherent in any dynamic model of the corona that terminates artificially at a given point in the solar atmosphere, it is of little concern (as a practical matter) if new flux is introduced in a region where the pre-existing field is quite weak compared to the field strength of the emerging structure. If, however, one wishes to study a case where magnetic flux emerges into the midst of a strong complex active region, the interaction of the emerging flux from below with pre-existing field that threads the boundary cannot be ignored.

Even if the models were truly coupled together (allowing for information exchange in both directions), it remains impractical to simultaneously model flux emergence with a combined domain that stretches from the convective overshoot layer to the low corona. Thus, we must make an approximation that will allow for the introduction of flux from the sub-surface calculation into a pre-existing coronal configuration, keeping in mind the physical limitations (or possible inconsistencies) of such an approximation. One method is to assume that photospheric flow dominates the boundary layer, and the dynamic back-reaction from coronal forces can be neglected. Then the ideal induction equation is linear, and if we express the magnetic field in the boundary layer as $\mathbf{B} \equiv \mathbf{B}_1 + \mathbf{B}_2$—a superposition of the quantities $\mathbf{B}_1$, which represents new flux introduced into the system from below (we require that $\mathbf{B}_1$ at $t = 0$ be zero), and $\mathbf{B}_2$, which at $t = 0$ represents the portion of the initial coronal flux system that permeates the boundary layer—we can recast the induction equation as

$$\frac{\partial}{\partial t}(\mathbf{B}_1 + \mathbf{B}_2) = \nabla \times \mathbf{v}_1 \times (\mathbf{B}_1 + \mathbf{B}_2) \tag{12}$$

here, $\mathbf{v}_1$ denotes the imposed boundary flow. Since $\partial \mathbf{B}_1/\partial t = \nabla \times \mathbf{v}_1 \times \mathbf{B}_1$ is satisfied for all time t ($\mathbf{v}_1$ and $\mathbf{B}_1$ are the velocity and magnetic field from the sub-surface MHD calculation used to drive the coronal model), we are left with the equations $\partial \mathbf{B}_2/\partial t = \nabla \times \mathbf{v}_1 \times \mathbf{B}_2$. This system can be used to advance $\mathbf{B}_2$, since the initial state $\mathbf{B}_2$ at $t = 0$ is known, and $\mathbf{v}_1$ is specified for all time t. Once $\mathbf{B}_2$ is determined for a given time step, the boundary field $\mathbf{B}$ can be updated in the usual way. A remaining question is how to properly evaluate the vertical derivatives of $\mathbf{B}_2$ in the zone below the boundary layer. We are currently experimenting with this technique using the ANMHD-ZEUS3D combined model of Abbett and Fisher (2003).

An alternative is to specify the same boundary conditions as described above for the initially field-free case. Namely, to specify $\mathbf{E}_t$ at $z = 0$ as determined from the sub-photospheric evolution code (which ignores the presence of the pre-existing coronal field), and also to set $\mathbf{v}$ at $z = 0$ in the same way. This will guarantee that B_z evolves correctly (i.e., B_z at the base of the corona will include the vertical component of the pre-existing coronal field, B_z^0, plus a contribution due to the emerging field, ΔB_z). The tangential magnetic field $\mathbf{B}_t$ will evolve due to $\mathbf{E}_t$ as well as due to E_z, the normal component of the electric field. This component of the electric field is advanced in time on the boundary $z = 0$ of the coronal solution, according to the equation $E_z = -(v_x B_y - v_y B_x)/c + \eta J_z$. Thus, E_z at $z = 0$ is not a boundary condition, it is a computed quantity. Since the evolution equation for E_z depends on the components of $\mathbf{B}_t$, the evolution of E_z will include the contribution of the pre-existing coronal magnetic field $\mathbf{B}_t^0$ at $z = 0$ (since $\mathbf{B}_t = \mathbf{B}_t^0 + \Delta \mathbf{B}_t$).

This approach represents an additional approximation to Eq. (12) and can alternately be expressed as

$$\frac{\partial \mathbf{B}}{\partial t} = \nabla \times (\mathbf{v}_1 \times \mathbf{B}_1) + \nabla \times [(\mathbf{v}_1 \times \mathbf{B}_2)\cdot\hat{\mathbf{z}} - \eta J_z]\hat{\mathbf{z}}. \tag{13}$$

In this approximation, we neglect the components of $\partial \mathbf{B}_2/\partial t = \nabla \times \mathbf{v}_1 \times \mathbf{B}_2$ that alter the prescribed evolution of B_z (i.e., $\hat{\mathbf{z}}\cdot\partial \mathbf{B}_2/\partial t$) or involve vertical gradients of $\mathbf{B}_2$. This scheme will work if the pre-existing coronal magnetic field has a negligible effect on the emergence of the sub-photospheric magnetic field. In reality, the coronal magnetic field may indeed affect the rise of sub-photospheric flux (i.e., coronal forces may modify the velocity determined from the sub-photospheric evolution). The extent to which the pre-existing coronal magnetic field affects the emergence of sub-photospheric flux is not known.

Using the approach just described (i.e., specification of $\mathbf{E}_t$ and $\mathbf{v}$ at $z = 0$), we have simulated the emergence of a twisted flux tube into a corona with a pre-existing large scale, bipolar background ("arcade-like") field. This initial arcade field is assumed to be potential. Two cases are considered: in the first case, the arcade field has opposite polarity to the emerging bipole; in the second case, the arcade field has the same polarity. The arcade field is chosen to be weaker than the emerging flux–tube field ($B_{\mathrm{flux-tube}} \approx 8 B_{\mathrm{arcade}}$), but distributed over a larger spatial scale ($L_{\mathrm{arcade}} \approx 8 L_{\mathrm{flux-tube}}$), so that the two flux systems have approximately the same net flux. Fig. 2 shows the evolution of the magnetic field for the first case (emergence into an opposite-polarity arcade). As the flux tube emerges into the corona, the field topology becomes quite complex. There is a neutral line (the white ribbon separating red and blue regions) that surrounds the emerged flux as well as cutting between the emerged opposite-polarity regions. Fig. 3 shows the evolution of

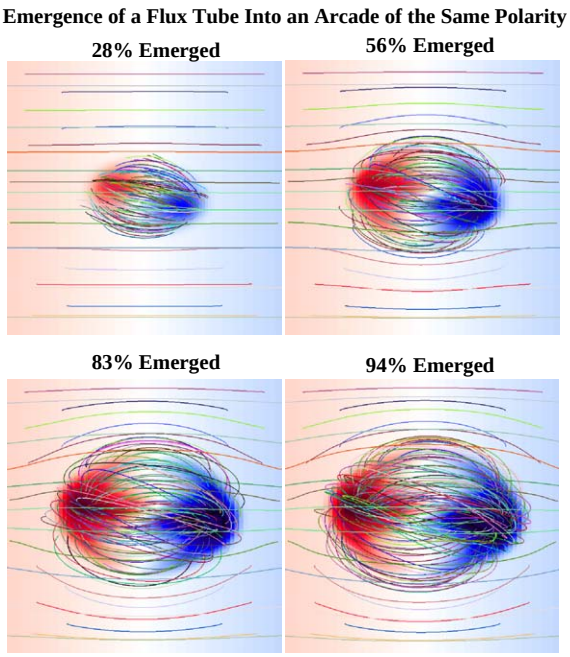

Fig. 3. Magnetic field evolution for a case where active-region magnetic flux emerges into a arcade of the same polarity. See text for details.

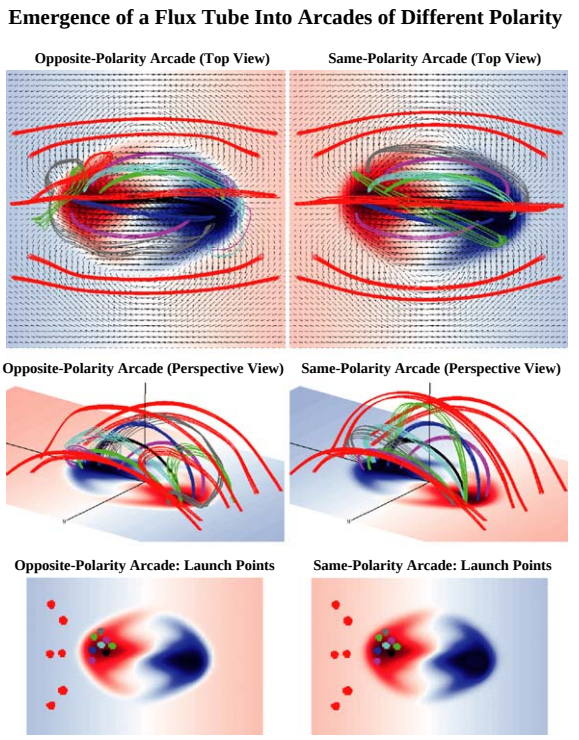

Fig. 4. A comparison of the topologies between the two cases shown in Figs. 2 and 3. See text for details.

the magnetic field for the second case (emergence into a same-polarity arcade).

The topology of selected bundles of field lines in the two configurations is compared in Fig. 4, at the instant at which the flux tube has emerged 83%. The top row shows a top view of the magnetic field lines, with colors at $z = 0$ representing B_z, and arrows representing $\mathbf{B}_t$. The middle row shows a perspective view of the field lines, and the bottom row shows the locations of the launch points for the field lines.

In the same-polarity field case, the topology is quite similar to the case in which there was initially no field in the corona (Fig. 1). In contrast, the field topology for the opposite-polarity emergence shows a complicated connectivity. This is not a surprise, since the field lines in the opposite-polarity case are expected to undergo reconnection as they emerge into an overlying field with the opposite orientation. Additionally, there appear to be field lines with "dipped" sections adjacent to the neutral line. Such field lines are interesting because they have the ability to support prominence material against gravity. The field lines in the gray bundle in the opposite-polarity panels of Fig. 4 show such dipped (concave-upward) shapes. Note also that the field lines in one of the green bundles clearly shows that reconnection has occurred in the opposite-polarity case, since its footpoints, which start in the boundary of the flux–tube core, connect to the flux in the overlying arcade. This is in contrast to the same-polarity case, in which these green field lines remain connected within the flux tube.

4. The initial atmosphere for data-driven models

If the coronal model is to be strictly data-driven, there are two distinct challenges that must be overcome: First, MHD codes require information about the velocity field as well as the vector magnetic field at the interface layer (e.g., finite volume algorithms require that the electric field along the edge of control volumes be specified so that the magnetic field can be advanced in time). For data-driven models, the flow field (or electric field) that is specified at the boundary must be consistent with the observed evolution of magnetic structures at the photosphere. For example, in an ideal calculation, any electric field imposed in the lower boundary layers must be derivable from a velocity field that satisfies the ideal induction equation (Eq. (10)), given the observed time evolution of the magnetic field (while simultaneously not over-specifying the MHD system of equations). Since the flow of magnetized plasma consistent with a given time series of vector magnetograms is an observational quantity that is generally unavailable, we note that the system of Eq. (10) is under-determined. Additionally, we have no observationally determined information

about the vertical gradients of the magnetic field in the boundary layers (necessary to properly update the transverse components of the magnetic field). To address these challenges new inversion techniques have recently been developed: Welsch et al. (2004) have presented a method that uses vector magnetic field measurements, along with local correlation tracking velocities (derived from the observed motion of magnetic elements) and the hypothesis of Démoulin and Berger (2003) to calculate a velocity field consistent with the observed time evolution of the magnetic field normal to the visible surface. Longcope (2004) take a different approach, and constrain the under-determined system by requiring that the plasma be in a minimum energy state.

Second, an MHD model corona requires the initial specification of the magnetic field throughout the computational volume, given the specification of the three components of the field at the photospheric boundary. In the context of data-driven models, one desires an initial magnetic topology that is as similar as possible to the topology inferred from X-ray observations of the corona above the active region of interest. Generally, active regions that are prone to eruptions are highly complex, and exhibit structures that often do not compare favorably to a local potential field extrapolation. We are thus forced to consider more computationally expensive techniques, and turn to non-constant-α force-free extrapolations as a means to generate an initial atmosphere. It is important to note that there are a number of ways to construct force-free equilibria (some more computationally expensive than others), but in general, each is sensitive to the prescribed boundary conditions, and can be less accurate near the photospheric boundary when the imposed boundary significantly differs from a force-free state. Methods that introduce significant differences in the value of the transverse components of the field at the photosphere from those prescribed by the magnetogram are generally unsuitable for use as starting atmospheres for dynamic calculations, since large unphysical gradients between the boundary zones and the first active zones result in unrealistic currents and Lorentz forces that can significantly affect a calculation.

We now examine a minimization technique proposed by Wheatland et al. (2000) to obtain force-free coronal field approximations. Briefly, this technique can be described in the following way: Let $\mathbf{B}(\mathbf{x}, t)$ be a magnetic field defined in a volume V. The optimization method minimizes the quantity

$$L = \int_V [B^{-2}|(\nabla \times \mathbf{B}) \times \mathbf{B}|^2 + |\nabla \cdot \mathbf{B}|^2] \, \mathrm{d}V. \tag{14}$$

If L is reduced to zero, then $(\nabla \times \mathbf{B}) \times \mathbf{B} = 0$ and $\nabla \cdot \mathbf{B} = 0$ everywhere in V, and $\mathbf{B}$ is force-free everywhere in V. If we assume that $\partial \mathbf{B}/\partial t = 0$ on the external boundary, then differentiating Eq. (14) with respect to t, and applying a number of vector identities yields

$$\frac{\mathrm{d}L}{\mathrm{d}t} = -2 \int_V \mu F^2 \, \mathrm{d}V. \tag{15}$$

Here $\mathbf{F}$ is a complicated function of the field $\mathbf{B}$, and it is assumed that the field is evolved according to $\partial \mathbf{B}/\partial t = \mu \mathbf{F}$, where $\mu > 0$ is an arbitrary function, usually set to unity. The numerical process is iterative; given an initial model for the field $\mathbf{B}(\mathbf{x}, 0)$, the function $\mathbf{F}$ is calculated, then the field is incremented by $\mu \mathbf{F} \delta t$. The objective function L is guaranteed to decrease for each iteration, and the process repeats until L stops decreasing.

Wheatland et al. (2000) tested the method against the non-constant-α force-free results of Low and Lou (1990) and found excellent agreement. For that comparison, however, all of the boundary conditions were known. In our case, only the lower, photospheric boundary condition (at $z = 0$) is known. The choice of the initial field is very important, since the value of $\mathbf{B}$ on the boundary does not change. We have done calculations for which the initial field is a potential field extrapolation using $B_z(z = 0)$, and also have used a linear force-free extrapolation. The results are substantially different for each case, given the same $\mathbf{B}(z = 0)$, since the value of $\mathbf{B}$ on the upper and side boundaries are different for the potential and linear force-free cases. We believe that, for solar magnetic fields, the field looks to be potential far from active regions. For this reason, we prefer to use a potential field extrapolation as an initial state for our force-free minimization procedure.

We wish to gain confidence in the ability of a given extrapolation technique to provide a suitable starting state for a dynamic, data-driven calculation. Toward this end, we use the 3D MHD simulation described in Section 2.2 to generate several synthetic magnetograms (at different heights in the atmosphere) for use as a lower boundary for a non-constant-α force-free extrapolation. The left-hand side of Fig. 5 shows the field lines of the final snapshot of a 3D MHD calculation of a twisted magnetic flux tube, initially positioned just below the photosphere, after it has emerged through the model chromosphere and transition region into the corona. The color table corresponds to the angle $\theta = \cos^{-1}|\mathbf{J} \cdot \mathbf{B}/(|\mathbf{J}||\mathbf{B}|)|$ along a given field line (θ is essentially a measure of how force-free the field is at a given point in the atmosphere)—bright cyan corresponds to a θ of zero, while bright magenta indicates a value of $\pi/2$ (black denotes $\theta = \pi/4$). Thus, the more blue the field line, the more force-free the atmosphere is at that location. The left half of Fig. 5 shows the entire computational domain, and it is clear that except for the layers near to and including the photosphere (the lower boundary of the image, where the field lines are anchored), the field is essentially force-free. The

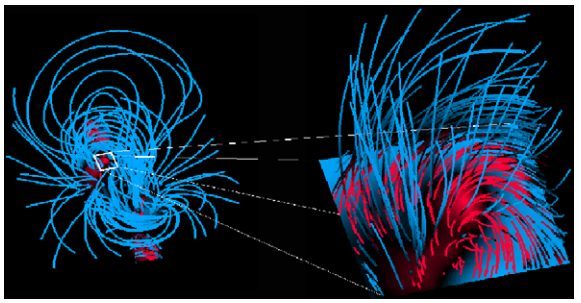

Fig. 5. Fieldlines from an MHD simulation of an emerging, twisted magnetic flux tube, the right-hand side of the image is a close-up of the boxed portion of the domain on the left-hand side. If a field line is cyan, the current is parallel to the field, and thus the atmosphere at that position is force-free; conversely if the field line is magenta, then this indicates that the current is perpendicular to the magnetic field, and the atmosphere at that position is not force-free. The simulation was performed on a $215 \times 167 \times 168$ non-uniform grid. See text for details.

right-hand side of Fig. 5 is a close-up of a portion of the domain near the lower boundary (the region indicated by the white box). This image demonstrates that the model atmosphere transitions from a highly non force-free configuration to a nearly force-free state in the chromospheric layers (the region where the red field lines transition into blue, several zones above the level denoted as the photospheric plane).

Fig. 6 shows the vertical (normal to the surface) component of the magnetic field (a synthetic magnetogram) for four levels in the model atmosphere: the upper-left frame represents a horizontal slice through the model photosphere, and the lower-right frame represents a horizontal slice through the model chromosphere. Dark areas represent regions of negative polarity ($B_z < 0$), while light areas denote regions of positive polarity ($B_z > 0$). Note that this single model active region produces synthetic magnetograms of distinctly different morphological characteristics, depending on the height where the magnetogram is generated—in the photosphere, portions of the twisted flux tube have yet to emerge, and in these areas, the transverse components of the magnetic field do not tend to fan out or converge radially at a given bipole, as one would expect to be the case after a portion of the flux rope has emerged into the low-density model corona (this is characteristic of the sub-surface simulations of Section 2.1 as well).

We now generate both potential field and non-constant-α force-free equilibria based on a synthetic photospheric magnetogram (top-left image in Fig. 6)—where the model atmosphere is not force-free, and portions of the flux rope have yet to fully emerge—and a synthetic chromospheric magnetogram (bottom-right image in Fig. 6), where the field approaches a force-free state. The results of these calculations are shown in

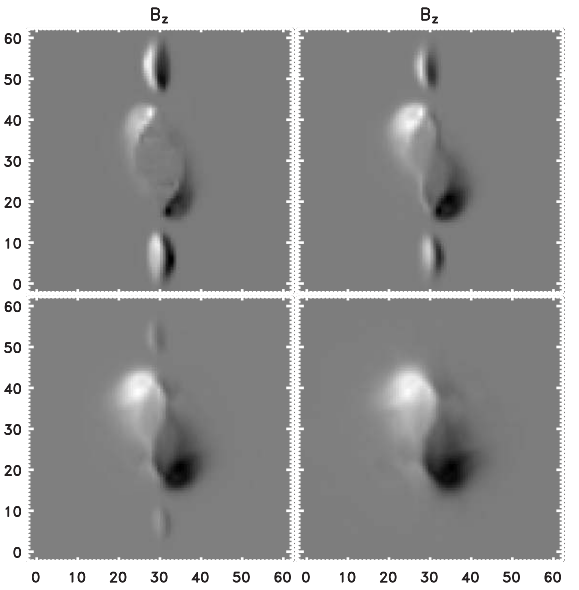

Fig. 6. A simulated vector "magnetogram"—the vertical component of the magnetic field along horizontal slices through an MHD simulation of emerging flux. The top-left image represents a slice through the model photosphere, and each successive image (left to right, top to bottom) represents a slice higher up in the atmosphere. The image on the bottom right is the vertical component of the field in a horizontal slice taken at a height corresponding to the model chromosphere. Not all of the computational domain is shown.

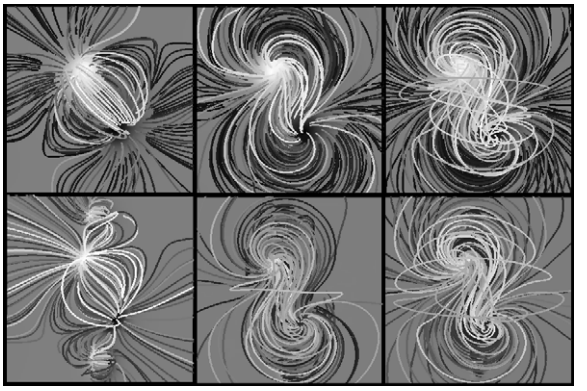

Fig. 7. Top row: a potential field (left) and non-constant-α force-free extrapolation (middle) based on the synthetic chromospheric magnetogram shown in the bottom-right frame of Fig. 6. Top right: the corresponding magnetic field lines for the MHD simulation. Bottom row: same as the top row for the photospheric magnetogram shown in the top-left frame of Fig. 6.

Fig. 7: the first column shows the magnetic structure resulting from a potential field extrapolation from both the chromospheric (top image) and photospheric (bottom image) lower boundaries. Similarly, the second column shows the magnetic structure resulting from a

non-linear force-free extrapolation, and the third column shows the magnetic structure of the fully dynamic MHD simulation (in each column, the top image corresponds to the chromospheric lower boundary, and the bottom image corresponds to the photospheric lower boundary). Not surprisingly, the potential field extrapolation does a poor job (in this case) of properly characterizing the magnetic topology of the simulation, since the emerging flux system is highly twisted. However, the non-constant-α extrapolation does remarkably well-reproducing the overall sigmoidal structure of the MHD model corona, though there are significant differences in the details. Such differences are to be expected, since an extrapolation cannot follow the continuous evolution of magnetic structures, during the dynamic emergence process.

To facilitate a comparison between the force-free extrapolation and the MHD calculation, the magnetic field along the external boundaries (the boundaries other than that boundary specified by the synthetic magnetogram) was taken to be identical to the field along the external boundaries of the MHD calculation. For an actual solar vector magnetogram, we do not have this luxury, and must specify the boundary via other means (a potential field is often used). We note that the resulting magnetic topology of the force-free model corona is highly dependent on the choice of boundary condition. For example, a potential external boundary, in our case, results in a poor match with the MHD results for the case where the photospheric lower boundary was used, though an extrapolation based on the chromospheric boundary fares somewhat better.

We now apply this method to an IVM vector magnetic field measurement of NOAA active-region 8210 (19:40 UT on May 1, 1998) provided by Régnier and Canfield (2003) at a moment just prior to a number of eruptive events. Although at the visible surface this is an extremely complex active region, and there is evidence from Yohkoh soft X-ray images of the global corona of a trans-equatorial connection between AR 8210 and AR 8214 (another large active region that is observed to flare concurrently with AR 8210, see e.g., Pevtsov, 2000), we nevertheless apply the Wheatland et al. (2000) method to a local domain surrounding only the CME-producing AR 8210. Yohkoh images of the corona above AR 8210 indicate that the coronal magnetic field well above the visible surface looks qualitatively potential (see e.g., Lundquist et al., 2003), thus we require that the external boundary conform to a potential configuration (we note that this does not preclude open field regions), and use the IVM vector magnetic field to specify the lower boundary and proceed with a non-constant-α force-free extrapolation in a Cartesian domain.

Fig. 8 shows the resulting force-free magnetic configuration at two different viewing angles for AR 8210. The

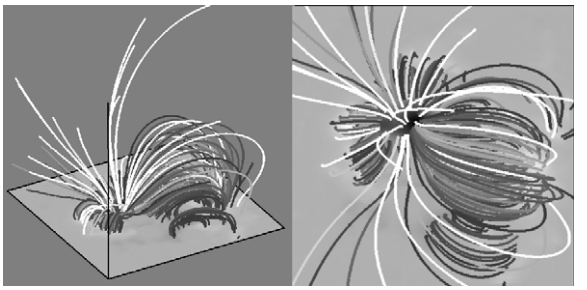

Fig. 8. Non-constant-α force-free extrapolation based on an IVM vector magnetogram of NOAA active-region 8210. Two different viewing angles are shown. The lighter the field line, the stronger the normal component of the magnetic field at the loop footpoint.

field lines are anchored in the photosphere, and the relative brightness or darkness of each individual field line corresponds to the strength of the normal component of the field at the photosphere—the brighter the line, the stronger the field at the loop footpoint. The left-hand image of Fig. 8 shows a number of open field lines that emanate close to a sheared magnetic neutral line that separates a large rotating negative polarity at the center of the active region from an emerging flux region. The open field lines (that leave the left-hand side of the box) overlie a closed arcade—we note that this 3D configuration is qualitatively similar to a 2D schematic presented by Sterling and Moore (2001) in an effort to characterize the observations and describe the physical process underlying the observed eruptive events and EIT emission. However, the only way to judge the relative success or failure of the extrapolation of Fig. 8 in describing AR 8210's coronal topology is to compare available X-ray images with the field lines of the calculation (where it is assumed hot X-ray emitted plasma will be confined). Qualitatively, the extrapolation compares reasonably well with the magnetic topology inferred from Yohkoh images of the corona above AR 8210 near the time of the magnetogram; namely, the three bright regions that appear in the soft X-ray images correspond with the three distinct closed loop systems evident in the right-hand image of Fig. 8, and the presence of open field anchored near the magnetic neutral line west of the large, central area of negative polarity active region corresponds to the prominent narrow dark feature at that same location in both soft X-ray and H-α images (see Sterling and Moore, 2001).

Of course, this type of comparison is qualitative at best, since there can be a number of interpretations of a given image, and a force-free extrapolation contains absolutely no information about plasma energetics (we note that Lundquist et al., 2003 have shown that it may be possible to theoretically reconstruct loop emission

once the magnetic topology is known, given a variety of assumptions about how the corona is heated). Thus, unless we make a number of assumptions regarding the thermodynamic properties of the coronal loops in the calculation, a direct, quantitative comparison between this calculation and the observed emission is not possible.

5. Discussion and conclusions

To a good approximation in the highly conducting corona, the magnetic field is "line-tied" to the photosphere, and evolves in response to changes in the magnetic field at the visible surface (see e.g., Schrijver and Title, 2001 for a striking example of how the corona responds to the rotating portion of NOAA active-region 9114 as seen by the TRACE satellite). By using codes such as ANMHD (or the model atmospheres of e.g., Magara and Longcope, 2003 or Bercik, 2002) to drive MHD models of the corona, it is possible to progress beyond highly idealized experiments, and investigate how the complex interaction of vector magnetic fields and flows at the lower boundary of a model corona affects the global evolution of magnetic structures. However, to progress beyond strictly theoretical calculations, it is essential to develop and test the techniques necessary to drive model coronae with photospheric or chromospheric *vector* magnetograms. We have coupled ANMHD and the SAIC models as an initial step in this effort.

We note that the code ANMHD is designed to model the dynamic evolution of magnetic structures below the visible surface of the Sun, while the SAIC model describes the evolution of magnetically dominated coronal plasma. In principle, ANMHD should be coupled to a stratified model atmosphere whose domain includes the entirety of the photosphere, chromosphere, transition region, and corona (see e.g., Abbett and Fisher, 2003; Magara and Longcope, 2001). However, we find that ANMHD is able to provide a physically self-consistent set of magnetic fields and flows suitable for incorporation as a boundary condition for the SAIC coronal model. We have successfully emerged a twisted Ω-loop (a flux rope where the central portion is more buoyant than the ends) into an initially field-free corona based on boundary conditions provided by ANMHD simulations, and have investigated the interaction of emerging fields with a pre-existing coronal structure. We have simulated the emergence of a current-carrying flux tube into a relatively strong, pre-existing potential coronal field, and have explored two different orientations of the pre-existing field with respect to the emerging structure. In future work, we plan to extend these results by considering the interaction between twisted emerging flux-tubes and initially twisted coronal fields.

Among the principal challenges of data-driven modeling is the specification of the 3D magnetized atmosphere that will be used to initiate a calculation. Since there is currently no means of directly measuring coronal magnetic fields, we must use available measurements of the magnetic field at the visible surface as a basis for an extrapolation. The results of these extrapolations must then be verified against soft X-ray images of the corona. Generally, dynamic active regions prone to eruption exhibit highly complex magnetic topologies that are not well described by a potential field. Since the CME initiation mechanism may depend on how the magnetic topology of the corona changes in time, a correct characterization of the pre-eruptive magnetic structure of the corona is a crucial component of our effort to simulate a magnetic eruption. We therefore use a non-constant-α force-free extrapolation to generate an initial magnetic configuration suitable to initiate a realistic, data-driven MHD model corona.

However, it has yet to be shown that a non-constant-α force-free extrapolation is mathematically unique (for a given set of boundary conditions). Additionally, we note that force-free solutions can be less accurate (depending on the numerical method used to obtain the result) near the lower boundary of the computational domain if the imposed lower boundary differs significantly from a force-free state (as can be the case in the photosphere). We have therefore tested the computationally inexpensive technique of Wheatland et al. (2000) against a fully compressible 3D MHD simulation of the emergence of a highly twisted magnetic flux tube (using the code of Magara, 1998) through the stratified layers of the photosphere, chromosphere and transition region into the corona. After the flux has fully emerged, we applied the Wheatland et al. (2000) method to two synthetic magnetograms: one generated by taking a slice through the MHD calculation at a height corresponding to the model photosphere, and one generated by taking a slice through the model chromosphere. We find that in both cases, the non-constant-α force-free extrapolations compare (qualitatively) quite well to the self-consistent MHD result, given that the magnetic field at the external boundaries matches that of the MHD simulation. We then applied this technique to NOAA AR 8210—a major eruptive active region. The extrapolation gave us a magnetic topology that compared favorably to Yohkoh soft X-ray images, while at the same time provided us with a 3D magnetic configuration whose magnetic fields match those specified by the IVM photospheric vector magnetogram.

Acknowledgements

The authors would like to thank Janet Luhmann, Brian Welsch, and Dave Bercik for useful comments and

discussion during the preparation of this manuscript. We would also like to thank Stephane Régnier and Dick Canfield for kindly providing us with vector magnetograms of AR 8210. This material is based upon work supported by: CISM, which is funded by the STC Program of the National Science Foundation under Agreement Number ATM-0120950, the DoD/AFOSR MURI grant "Understanding Magnetic Eruptions and their Interplanetary Consequences", NASA's Sun-Earth Connection Theory Program and Supporting Research & Technology Program, NASA Contract NAS 5-98033, and NSF Grant ATM-0327712.

References

Abbett, W.P., Fisher, G.H., 2003. A coupled model for the emergence of magnetic flux into the solar corona. The Astrophysical Journal 582 (1), 475–485.

Abbett, W.P., Fisher, G.H., Fan, Y., 2000. The three-dimensional evolution of rising, twisted magnetic flux tubes in a gravitationally stratified model convection zone. The Astrophysical Journal 540 (1), 548–562.

Abbett, W.P., Fisher, G.H., Fan, Y., 2001. The effects of rotation on the evolution of rising omega loops in a stratified model convection zone. The Astrophysical Journal 546 (2), 1194–1203.

Aly, J.J., 1991. How much energy can be stored in a three-dimensional force-free magnetic field? The Astrophysical Journal 375 (2), L61–L64.

Amari, T., Aly, J.J., Luciani, J.F., Boulmezaoud, T.Z., Mikić, Z., 1997. Reconstructing the solar coronal magnetic field as a force-free magnetic field. Solar Physics 174 (1), 129–149.

Amari, T., Luciani, J.F., Aly, J.J., Mikić, Z., Linker, J., 2003. Coronal mass ejection: initiation, magnetic helicity, and flux ropes. I. boundary motion-driven evolution. The Astrophysical Journal 585 (2), 1073–1086.

Antiochos, S.K., Devore, C.R., Klimchuk, J.A., 1999. A model for solar coronal mass ejections. The Astrophysical Journal 510 (1), 485–493.

Bercik, D.J., 2002. A numerical investigation of the interaction between convection and magnetic field in a solar surface layer. Ph.D. Thesis, Michigan State University.

Bineau, M., 1972. Existence of force-free magnetic fields. Communications on Pure and Applied Mathematics 25 (1), 77.

Bleybel, A., Amari, T., van Driel-Gesztelyi, L., Leka, K.D., 2002. Global budget for an eruptive active region. I. equilibrium reconstruction approach. Astronomy and Astrophysics 395, 685–695.

Canfield, R.C., Hudson, H.S., McKenzie, D.E., 1999. Sigmoidal morphology and eruptive solar activity. Geophysical Research Letters 26 (6), 627.

Casini, R., López Ariste, A., Tomczyk, S., Lites, B.W., 2003. Magnetic maps of prominences from full Stokes analysis of the He I D3 line. The Astrophysical Journal 598 (1), L67–L70.

Démoulin, P., Berger, M.A., 2003. Magnetic energy and helicity fluxes at the photospheric level. Solar Physics 215 (2), 203–215.

Fan, Y., 2001. The emergence of a twisted Ω-tube into the solar atmosphere. The Astrophysical Journal 554 (1), L111–L114.

Fan, Y., Gibson, S.E., 2003. The emergence of a twisted magnetic flux tube into a pre-existing coronal arcade. The Astrophysical Journal 589 (2), L105–L108.

Fan, Y., Zweibel, E.G., Linton, M.G., Fisher, G.H., 1999. The emergence of kink-unstable magnetic flux tubes and the origin of delta-configuration sunspots. The Astrophysical Journal 521 (1), 460–477.

Feynman, J., Martin, S.F., 1995. The initiation of coronal mass ejections by newly emerging magnetic flux. Journal of Geophysical Research 100 (A3), 3355–3367.

Forbes, T.G., Isenberg, P.A., 1991. A catastrophe mechanism for coronal mass ejections. The Astrophysical Journal 373 (1), 294–307.

Gough, D.O., 1969. The anelastic approximation for thermal convection. Journal of Atmospheric Science 26, 448–456.

Kuhn, J.R., MacQueen, R.M., Streete, J., Tansey, G., Mann, I., Hillebrand, P., Coulter, R., Lin, H., Edmunds, D., Judge, P., 1999. Probable detection of a bright infrared coronal emission line of Si IX near 3.93 microns. The Astrophysical Journal 521 (1), 478–482.

Lantz, S.R., Fan, Y., 1999. Anelastic magnetohydrodynamic equations for modeling solar and stellar convection zones. The Astrophysical Journal Supplement Series 121 (1), 247–264.

Lee, J., McClymont, A.N., Mikić, Z., White, S.M., Kundu, M.R., 1998. Coronal currents, magnetic fields, and heating in a solar active region. The Astrophysical Journal 501, 853.

Lee, J., White, S.M., Kundu, M.R., Mikić, Z., McClymont, A.N., 1999. A test for coronal magnetic field extrapolations. The Astrophysical Journal 510 (1), 413–421.

Lin, H., Penn, M.J., Tomczyk, S., 2000. A new precise measurement of the coronal magnetic field strength. The Astrophysical Journal 541 (2), L83–L86.

Linker, J.A., Mikić, Z., 1997. The initiation of coronal mass ejections by magnetic shear. In: Crooker, N., Joselyn, J., Feynman, J. (Eds.), Coronal Mass Ejections, Geophysical Monograph Series 99. American Geophysical Union, Washington DC, p. 269.

Lionello, R., Mikić, Z., Linker, J.A., 1999. Stability of algorithms for waves with large flows. Journal of Computational Physics 152 (1), 346–358.

Lionello, R., Linker, J.A., Mikić, Z., 2001. Including the transition region in models of the large-scale solar corona. The Astrophysical Journal 546 (1), 542–551.

Lionello, R., Mikić, Z., Linker, J.A., Amari, T., 2002. Magnetic field topology in prominences. The Astrophysical Journal 581 (1), 718–725.

Liu, Y., Zhao, X.P., Hoeksema, J.T., Scherrer, P.H., Wang, J., Yan, Y., 2002. On formation of the sigmoidal structure in solar active region NOAA 8100. Solar Physics 206 (2), 333–346.

Longcope, D.W., 2004. Inferring a photospheric velocity field from a sequence of vector magnetograms: the minimum energy fit. The Astrophysical Journal, in press.

Low, B.C., Lou, Y.Q., 1990. Modeling solar force-free magnetic fields. The Astrophysical Journal 352, 343–352.

Luhmann, J.G., Li, Y., Arge, C.N., Gazis, P.R., Ulrich, R., 2002. Solar cycle changes in coronal holes and space

weather cycles. Journal of Geophysical Research (Space Physics) 107 (A8), 1154.

Lundquist, L.L., Fisher, G.H., Régnier, S., Liu, Y., Abbett, W.P., 2003. Temperature, density, and magnetic field reconstructions of active region coronae. AGU Fall Meeting Abstracts, pp. 509.

Lyon, J., Goodrich, C., Sussman, A., Andrade, H., Wiltberger, M., 2003. A general code coupling framework and the dissection of the LFM code. American Geophysical Union Fall Meeting 2003 Abstracts, SM22A-0222.

MacNeice, P., Olson, K.M., Mobarry, C., deFainchtein, R., Packer, C., 2000. PARAMESHA: a parallel adaptive mesh refinement community toolkit. Computer Physics Communications 126, 330.

Magara, T., 1998. Ph.D. Thesis, University of Kyoto.

Magara, T., 2004. A model for the dynamic evolution of emerging magnetic fields in the Sun. The Astrophysical Journal 605 (1), 480–492.

Magara, T., Longcope, D.W., 2001. Sigmoid structure of an emerging flux tube. The Astrophysical Journal 559 (1), L55–L59.

Magara, T., Longcope, D.W., 2003. Injection of magnetic energy and magnetic helicity into the solar atmosphere by an emerging magnetic flux tube. The Astrophysical Journal 586 (1), 630–649.

McClymont, A.N., Jiao, L., Mikić, Z., 1997. Problems and progress in computing three-dimensional coronal active region magnetic fields from boundary data. Solar Physics 174 (1), 191–218.

Mikić, Z., Linker, J.A., 1994. Disruption of coronal magnetic field arcades. The Astrophysical Journal 430 (2), 898–912.

Mikić, Z., McClymont, A.N., 1994. Deducing coronal magnetic fields from vector magnetograms. In: Balasubramaniam, K.S., Simon, G.W. (Eds.), Solar Active Region Evolution: Comparing Models with Observations, ASP (Astronomical Society of the Pacific) Conference Series 68, p. 225.

Mikić, Z., Linker, J.A., Schnack, D.D., 1996. Global coronal modeling and space weather prediction. In: Balasubramaniam, K.S., Keil, S.L., Smartt, R.N. (Eds.), Solar Drivers of Interplanetary and Terrestrial Disturbances ASP (Astronomical Society of the Pacific) Conference Series 95, p. 108.

Mikić, Z., Linker, J.A., Schnack, D.D., Lionello, R., Tarditi, A., 1999. Magnetohydrodynamic modeling of the global solar corona. Physics of Plasmas 6 (5), 2217–2224.

Mok, Y., Mikić, Z., Linker, J.A., 2001. Interaction of two magnetic loops in the solar corona. The Astrophysical Journal 555 (1), 440–447.

Ogura, Y., Phillips, N.A., 1962. Scale analysis of deep and shallow convection in the atmosphere. Journal of Atmospheric Science 19, 173–179.

Pevtsov, A.A., 2000. Transequatorial loops in the solar corona. The Astrophysical Journal 531 (1), 553–560.

Régnier, S., Canfield, R.C., 2003. The active region 8210: observations, coronal magnetic fields and energetics. AGU Fall Meeting Abstracts, A174.

Régnier, S., Amari, T., Kersalé, E., 2002. 3D coronal magnetic field from vector magnetograms: non-constant-alpha force-free configuration of the active region NOAA 8151. Astronomy and Astrophysics 392, 1119–1127.

Schmidt, H.U., 1964. . In: Hess, W.N. (Ed.), Physics of Solar Flares, NASA SP 50, p. 107.

Schrijver, C.J., Title, A.M., 2001. . In: Svestka, Z., Engvold, O., Harvey, J.W. (Eds.), Solar Physics 200 (1), CDROM.

Stein, R.F., Nordlund, Å., 1998. Simulations of solar granulation. I. general properties. The Astrophysical Journal 499, 914.

Stein, R.F., Bercik, D., Nordlund, Å., 2003. . In: Current Theoretical Models and Future High Resolution Solar Observations: Preparing for ATST. ASP Conference Series 286, p. 121.

Sterling, A.C., Moore, R.L., 2001. EIT crinkles as evidence for the breakout model of solar eruptions. The Astrophysical Journal 560 (2), 1045–1057.

Tomczyk, S., 2003. Multi-channel polarimeter for coronal magnetic field measurements. American Geophysical Union Fall Meeting 2003 Abstracts, SH42D-03.

Welsch, B.T., Fisher G.H., Abbett, W.P., Régnier, S., 2004. ILCT: Recovering photospheric velocities from magnetograms by combining the induction equation with local correlation tracking. The Astrophysical Journal 610 (2), 1148–1156.

Wheatland, M.S., Sturrock, P.A., Roumeliotis, G., 2000. An optimization approach to reconstructing force-free fields. The Astrophysical Journal 540 (2), 1150–1155.